Dalton Transactions

PAPER

View Article Online
View Journal | View Issue

Cite this: *Dalton Trans.*, 2016, **45**, 6920

Red-light activated photoCORMs of Mn(I) species bearing electron deficient 2,2′-azopyridines†

E. Kottelat, A. Ruggi* and F. Zobi*

Received 3rd March 2016,
Accepted 3rd March 2016

DOI: 10.1039/c6dt00858e

www.rsc.org/dalton

The realization of CO releasing molecules triggered by light (photoCORMs) within the phototherapeutic window (λ > 600 nm) constitutes an important goal for potential therapeutic applications of the molecules. The activation of photoCORMs with red/NIR light would enable exploiting the higher depth of penetration of this radiation with respect to higher energy photons. In this article we report a family of carbonyl Mn(I) complexes capable of releasing CO when triggered with red light (≥625 nm). Such complexes are based on 2,2′-azopyridine ligands modified by the introduction of electron-donating or electron-withdrawing substituents. Our results indicate that electron deficient ligands induce a gradual decrease of the HOMO–1/LUMO gap of the species (*i.e.* of the orbitals involved in the lowest energy transition), thus enabling a fine tuning of their visible absorption maxima between 630 and 693 nm. The synthesis of the complexes and their photodecomposition behaviour towards CO release are described. We suggest that this approach could be generalized for further development of low-energy activated photoCORMs.

Introduction

Since the seminal discovery that carbon monoxide is implicated in different biological signalling pathways, different molecules capable of releasing CO (CORMs) have been reported.[1–5] These include a variety of organometallic complexes which are able to liberate CO by thermal activation or hydrolysis in biological media. For potential therapeutic applications of CORMs, temporal and spatial control of CO delivery is highly desirable. This may be achieved with compounds activated by external stimuli,[6–8] *e.g.* light. The latter class of molecules is known as photoactivated CORMs (photoCORMs).[9–11] Systems triggered by visible light still constitute a great challenge in the design of these molecules. Indeed, most of the known photoCORMs, with few exceptions, are activated with UV light.[12–17]

In particular the group of Mascharak has endeavoured to develop rational strategies to visible light-activated CORMs and has introduced carbonyl Mn(I) complexes with conjugated ligands showing MLCT bands in the visible region.[18–22] Their strategy is based fundamentally on two approaches, namely: (a) increasing the conjugation of bidentate aromatic ligands (thereby inducing a stabilization of the LUMO associated with the MLCT) and (b) substituting π-acid ancillary ligands with σ-donors or π-basic ligands (thereby increasing the HOMO–2 energy, the orbital involved in the lowest energy transitions). Upon applications of these strategies, carbonyl Mn(I) complexes with conjugated ligands of the 2-pyridyl-*N*-(2-methylthiophenyl)methylenimine and 2-phenylazopyridine types were designed. The latter complexes show MLCT bands with a maximum at *ca.* 585 nm, which constitutes the best result achieved so far in the field of stable photoCORMs activated with visible light.[18–22]

On the basis of these results and analogous effects observed in luminescent transition metal complexes,[23,24] we developed a new strategy for the design of photoCORMs absorbing in the red region of the visible spectrum. Our approach is based on *fac*-$[Mn(CO)_3]^+$ complexes bearing electron deficient 2,2′-azopyridines (azpy). The design of the ligands was developed starting from the benchmark (2-phenyldiazenyl)pyridine Mn(I) complex reported by the group of Masharak (λ_{max} = 586 nm). The bidentate ligand was modified by replacing the phenyl ring with a second pyridine to lower the energy of the π* MO of the –N=N– moiety, given the higher electronegativity of N compared to C. Moreover, the electronic density of the ligand was decreased by addition of electron withdrawing groups (EWG) on the ligand π-frame, to further stabilize the LUMO of the complexes and thus to shift the absorption of the MLCT to longer wavelengths.

The theoretical framework of our approach rests on the consideration that in complexes where CO photolability is

Département de Chimie, Université de Fribourg, Chemin du Musée 9, CH-1700 Fribourg, Switzerland. E-mail: albert.ruggi@unifr.ch, fabio.zobi@unifr.ch

† Electronic supplementary information (ESI) available: Crystallographic details, ^1H and ^{13}C NMR spectra of ligands and complexes and UV-Vis absorption spectra. CCDC 1430146–1430149 and 1446608. For ESI and crystallographic data in CIF or other electronic format see DOI: 10.1039/c6dt00858e

associated with MLCT (and consequent decrease of M–CO π* back bonding) electron withdrawing substituents on the ligand π-frame should further decrease the LUMO energy thereby reducing the HOMO–LUMO gap. This line of thought is corroborated by the fact that ligation of CO to a metal centre is assisted by metal-to-CO π-back bonding. Thus transfer of electron density from the metal centre to the π* MO of the ligand will be facilitated in electron poor (or deficient) π-ligands and therefore will further promote the labilization of the same M–CO bond.

Although it might appear trivial, this approach is counter-intuitive on the basis of what has been reported so far. In fact, addition of electron donating substituents on π-ligands was reported to red shift the MLCT transition of *fac*-$[Mn(CO)_3]^+$ complexes,[22,25] whilst the addition of electron deficient pyridine N donors in the ligand frame resulted in a blue shift of the MLCT.[18,19]

In this contribution we report the synthesis, characterization and photochemical behaviour of a family of electron deficient $[MnBr(azpy)(CO)_3]$ derivatives, providing experimental evidence for the realization of red-light activated photo-CORMs. The systematic substitution of 2,2′-azopyridine with weak donating to strong deactivating substituents (*i.e.* EWG) leads to the progressive bathochromic shift of the MLCT absorption band maximum from 625 nm to 693 nm (Fig. 1), enabling fine tuning of the absorption in the red region of the visible spectrum. Exposure of solutions of complexes **1–5** to low-power visible light (≥625 nm, formally red light) resulted in CO photorelease as evidenced by the myoglobin (Mb) assay.[26,27] Furthermore, the MLCT band of complexes with strong EWG tails beyond the visible region of the spectrum in the near infrared and in one case photodecomposition could also be triggered at 810 nm.

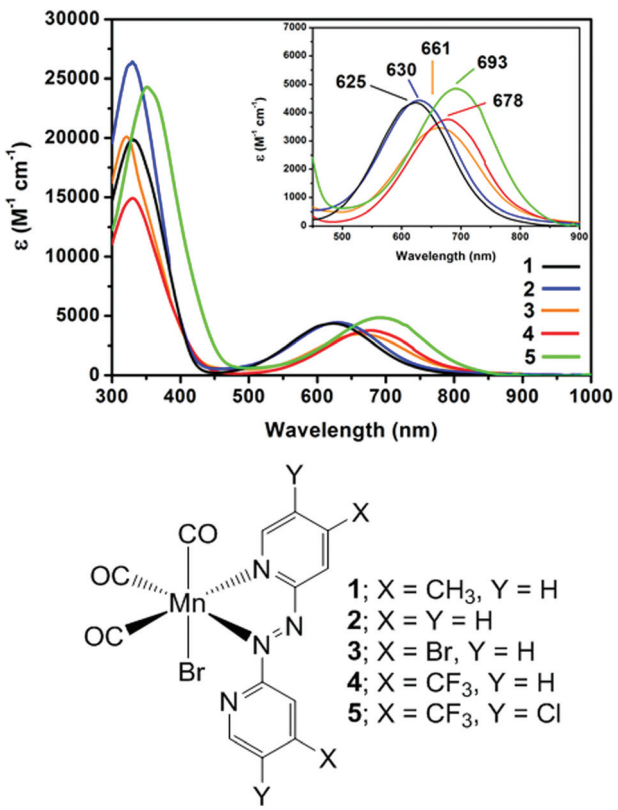

Fig. 1 Electronic absorption spectra (top) and the molecular structure of $[MnBr(azpy)(CO)_3]$ species presented in this work.

Results and discussion

Synthesis and characterization

The synthesis of Azpy_H is reported in the literature.[28] Such a method is based on the oxidation of aminopyridine with an aqueous solution of NaClO at 0 °C. However, we observed that this procedure gives only poor yields when applied to aminopyridines bearing electron-withdrawing and electron donating substituents. In fact, under these conditions, substituted aminopyridines give mixtures of chlorinated azopyridines with an overall yield <5%. The poor yield and the formation of chlorinated products are probably due to the poor water solubility of substituted aminopyridines together with the strong chlorinating power of NaClO. To overcome this problem, several mild oxidation methods were tried. In particular, we focused our attention on two reported methodologies, namely the use of *t*-BuClO in the presence of NaI (giving *in situ* formation of the mild oxidant *t*-BuIO), and the use of sodium dichloroisocyanurate.[29,30] However, in spite of the good solubility of our substrates in the solvents used for these methodologies (*e.g.* acetonitrile, THF), no formation of an azo group was observed. Therefore, a modification of the procedure based on NaClO was developed. The substrates were first dissolved in THF, followed by addition of aqueous NaClO at room temperature and evaporation of the organic solvent under vacuum. The resulting suspension turned red within minutes and was stirred overnight at room temperature giving a mixture of products (overall yields in the order of 20%) formed by the target azopyridine derivative together with monochlorinated and bischlorinated azopyridines which were separated by chromatography. Single crystals of Azpy_H were obtained upon slow diffusion of petroleum ether into a diethylether solution of the ligand. Single crystals of Azpy_Br, Azpy_CF_3 and Azpy_CF_3Cl were obtained upon slow evaporation of acetonitrile solutions (Fig. 2).

Complexes **1–5** were synthesized at room temperature in the dark by reacting three equivalents of $[MnBr(CO)_5]$ with one equivalent of the corresponding azpy ligand in dichloromethane (DCM), the excess of Mn(I) being required to circumvent the low thermal stability of complexes **3–5** (*vide infra* and ESI†). Blue single crystals of **2** were obtained in the dark by slow diffusion of hexane in a DCM solution. The coordination geometry of the Mn(I) centre is distorted octahedral with three CO ligands disposed facially (Fig. 3). In the structure, the N–N distance of the azo group is analogous to the related *fac*-[MnBr(L)$(CO)_3$] complex (where L = 2-phenylazopyridine) indicating a similar *d*(Mn) → azo(π*) back-bonding.[18,20] When crystalliza-

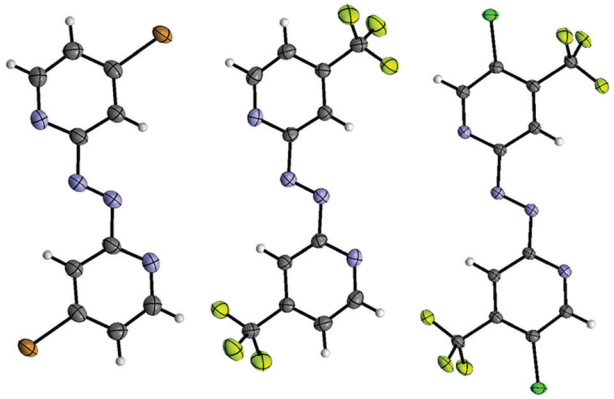

Fig. 2 Molecular structures of (from left to right) Azpy_Br, Azpy_CF_3, Azpy_CF_3Cl ligands. Thermal ellipsoids are shown at 30% probability.

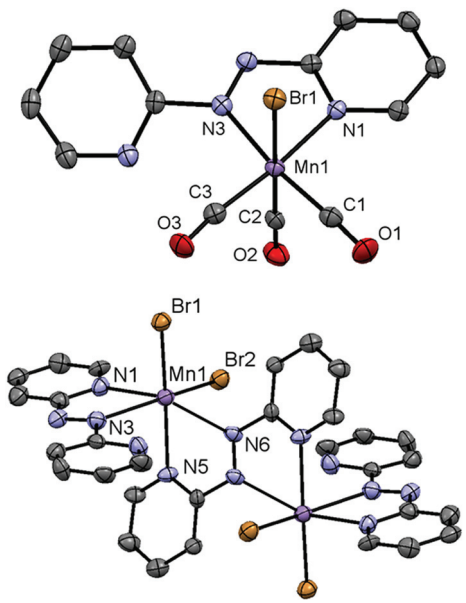

Fig. 3 Molecular structures of **2** (top) and its photodecomposition product (**2a**). Thermal ellipsoids are shown at the 30% probability level and the hydrogen atoms are omitted for clarity. Selected bond distances (Å) are for **2**: Mn–N1 2.014 (2), Mn–N3 2.007 (2), Mn–C1 1.805 (3), Mn–C2 1.806 (3), Mn–C3 1.829 (3), Mn–Br 2.5206 (5), N2–N3 (azo) 1.271 (3); for **2a**: Mn–N1 2.335 (9), Mn–N3 2.385 (11), Mn–N5 2.278 (9), Mn–N6 2.536 (9), Mn–Br1 2.546 (2), Mn–Br2 2.571 (2), N2–N3 (azo) 1.266 (14).

tion attempts of **2** were performed in ambient light, dark-brown needles of the paramagnetic Mn(II) $[Mn_2Br_4(azpy)_3]$ dimer (**2a**, Fig. 3) formed. The most obvious feature of this photodecomposition product is the complete loss of the carbonyl ligands. The metric parameters of **2a** are significantly different when compared to **2**. The Mn–N# distances in **2a** (where N# = N1 and N3) are on average >0.3 Å longer than the same in **2**. Likewise, the Mn–N distances for the bridging azpy ligand are elongated by *ca*. 0.3 (Mn–N5) and 0.5 (Mn–N6) Å.

Complex **2** displays ^{1}H and ^{13}C NMR spectra consistent with the diamagnetic ground state of Mn(I) centers (Fig. 4).

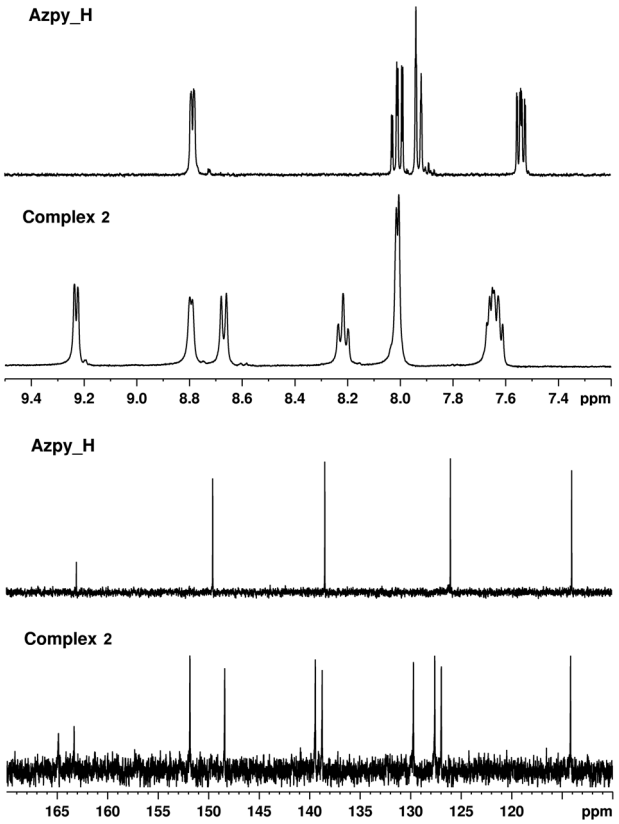

Fig. 4 ^{1}H- (top) and ^{13}C-NMR of ligand Azpy_H and its corresponding Mn(I) complex (**2**) showing the loss of the magnetic homotopic nature of the azpy ligand upon coordination to the metal centre.

The magnetic homotopic nature of the azpy ligand is lost upon coordination to the metal giving two sets of resonances for bound and free pyridines. Analogous effects are observed in the ^{1}H and ^{13}C NMR spectra of **1**, and **3–5** (ESI†). On the basis of this spectroscopy analysis we assign a similar coordination of the substituted azpy ligands in species**1**, and **3–5**.

Electronic spectroscopy

Solutions of **1–5** in dichloromethane exhibit two strong absorption bands (Fig. 1 and Table 1). A maximum in the 320–350 nm range ascribed to an azpy $\pi \rightarrow \pi^*$ transition and a band in the visible region (λ_{max} (vis.) in Table 1). The absorption maxima of the low-energy bands in dichloromethane appear at 625 nm for **1**, 630 nm for **2**, 661 nm for **3**, 678 nm for **4**, and 693 nm for **5**. The high molar absorptivities of these bands indicate that they may be assigned to charge transfer transition(s).[18–20,22] This assignment was further confirmed by TD-DFT calculations (Fig. 5). Such calculations show in all cases that the most prominent low-energy transition in the visible (λ_{max} (vis.)) is a HOMO−1 → LUMO. As is evident from the orbital diagrams shown in Fig. 5, HOMO−1 has predominantly a π(Br) and a *d*(Mn) character, whilst LUMO has mostly a π-azpy character. Moreover, the orbital splitting of the HOMO−1 → LUMO transition is strongly influenced by the electronic character of the *para*-substituents (ESI†). In fact, the

Table 1 Spectroscopy details and half-life ($t_{1/2}$) for the thermal- and photo-decomposition of species **1–5**

			$t_{1/2}$ (h, in DCM)[a]			$t_{1/2}$ (h, Mb assay)[b]	
Species	λ UV-Vis (nm)	ε (M^{-1}, cm^{-1}) × 10^{-3}	Dark	λ_{max} (vis.)	810 (nm)	Dark	λ_{max} (vis.)
1	329, 625	19.86, 4.35	n.d.	3.52 ± 0.06	n.d.	n.d.	1.50 ± 0.05
2	330, 630	26.42, 4.43	n.d.	3.60 ± 0.05	n.d.	n.d.	1.13 ± 0.17
3	322, 661	20.09, 3.46	3.05 ± 0.30	1.21 ± 0.14	2.92 ± 0.16	0.85 ± 0.11	0.76 ± 0.05
4	331, 678	14.91, 3.76	1.07 ± 0.02	0.48 ± 0.01	1.04 ± 0.08	0.50 ± 0.05	0.21 ± 0.01
5	351, 693	24.3, 4.85	1.23 ± 0.03	0.41 ± 0.01	0.65 ± 0.07	0.54 ± 0.07	0.31 ± 0.01

[a] n.d. = not determined, *i.e.* $t_{1/2}$ > 4 h. [b] n.d. = not determined, *i.e.* <0.1 eq. CO released.

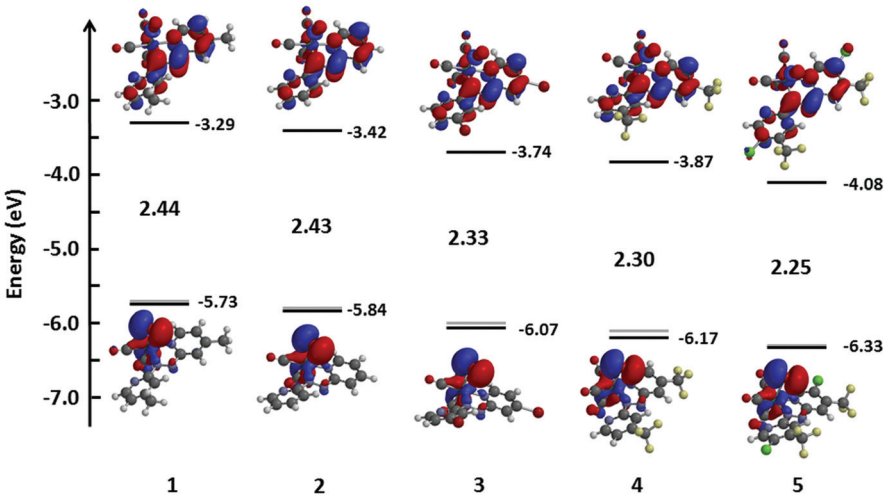

Fig. 5 Calculated HOMO–1 and HOMO/LUMO energy diagram of complexes **1–5**. The most prominent MOs involved with transitions under the low-energy band and their diagrams are shown (the orbitals in TD-DFT calculations are also shown).

introduction of a EWG, with respect to the pristine complex **2**, induces a decrease of the orbital splitting.

This variation, predicted by DFT calculations, is in excellent agreement with the experimental position of λ_{max} (vis.).

The relative position of λ_{max} (vis.) in **1–4** increases as a function of the azpy-X *para*-substituent (see Fig. 1) from $-CH_3$ (625 nm) to $-CF_3$ (678 nm). Additional substitution of the *para*-CF_3 π-ligand with *meta*-Cl further increases λ_{max} (vis.) in **5** by 15 nm (*i.e.* to 693 nm). The relative shift of these transitions is in excellent linear agreement with the values of the corresponding Hammett's parameters of the azpy substituents (R^2 = 0.98, ESI†) suggesting that the parameters may be used in this class of molecules to fine-tune λ_{max} (vis.).

Stability and CO releasing properties

In DCM **1** and **2** are stable for hours in the absence of light. Conversely, complexes **3–5** exhibit slow decomposition kinetics at room temperature as evidenced by the hypochromic shift of λ_{max} (vis.). To evaluate the half-life ($t_{1/2}$) of this process a kinetic analysis was performed by recording UV-Vis spectra as a function of time (Fig. 6). In all cases spectral changes are characterised by a decrease of the MLCT band and a hypsochromic shift of the azpy π → π* transition. In DCM **3–5** show a first order exponential degradation kinetic with $t_{1/2}$ in the dark of *ca.* 3 hours for **3** and 1 hour for **4** and **5** (Table 1, ESI†). When DCM solutions of **1–5** are irradiated at λ_{max} (vis.) faster decomposition kinetics are measured. Compounds **1** and **2** gave a photodecomposition $t_{1/2}$ of *ca.* 3.5 hours while **3–5** gave a $t_{1/2}$ value roughly equal to 1/3 of the same measured in the dark. The spectral changes exhibit distinct isosbestic points implying clean conversion to the corresponding photoproducts.

The MLCT band of complexes **3–5** tails beyond the visible region of the spectrum in the near infrared region (NIR). If photodecomposition of these species is triggered at 810 nm, only **5** reveals an increase in the photodecomposition kinetics. In this case $t_{1/2}$ is *ca.* half the dark reference value (*i.e.* 0.65 *vs.* 1.23 hours, see Table 1). This result is particularly significant as **5** is the first example of a photoCORM directly activated with NIR radiation, *i.e.* without using upconversion techniques.[31]

The photodecomposition of **1–5** is accompanied by CO release as established *via* the Mb assay (ESI†). If kept in the dark **1** and **2** released <0.1 equivalent of CO (determined from ε value of the Soret band of MbCO) while **3–5** on average *ca.* 0.7 equivalent within a 3 hours monitoring period. Under the

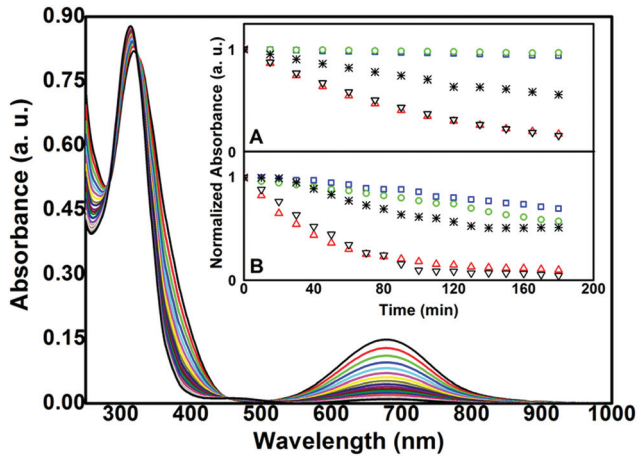

Fig. 6 Electronic absorption spectrum of **4** exemplifying the typical decay of the species herein described. Insert shows the kinetics of decomposition of DCM solutions of the complexes in the dark (A) and upon photoirradiation at λ_{max} (vis.) (B). Symbol keys: **1** (green ○), **2** (blue □), **3** (✱), **4** (red △), **5** (▽).

same conditions, photoirradiation of the complexes at λ_{max} (vis.) promoted rapid CO saturation of Mb. Generally speaking the $t_{1/2}$ values for this process are faster than the same photodecomposition kinetics measured in DCM (Table 1). The half-life of MbCO formation decreased steadily as a function of the azpy-substituents (varying from 1.50 for **1** to 0.31 hours for **5**, Table 1) suggesting a correspondence between $t_{1/2}$ and λ_{max} (vis.) and the thermal stability of the species.

Conclusions

In summary, we have described a new strategy for the realization of Mn(I)-azopyridine photoCORMs which can be excited with low-power red light (≥625 nm). The introduction of electron-donating and electron-withdrawing groups on the azopyridine ligand enables to finely tune the absorption of the complexes between 625 and 693 nm. TD-DFT calculations and UV-Vis spectroscopy show that, with respect to the pristine azopyridine complex **2**, the presence of the electron-withdrawing substituents induces a decrease of the HOMO−1/LUMO gap (*i.e.* of the orbitals involved in the lowest energy transition), with a consequent bathochromic shift of the visible absorption band of complexes **3**–**5**. Conversely, the introduction of electron-donating substituents (complex **1**) induces an increase of the HOMO−1/LUMO gap, with a consequent hypsochromic shift of the visible absorption band. All complexes have been analysed by ^{1}H and ^{13}C-NMR spectroscopy, which shows the presence of two sets of signals, belonging to bound and unbound pyridines. In the case of complex **2**, the structure proposed on the basis of NMR spectroscopy is further corroborated by the crystal structure obtained by X-ray diffraction of a single crystal. All complexes show photodecomposition upon irradiation with low power light at a wavelength corresponding to the visible absorption maxima, with the half-life varying between 3.5 and 0.41 hours. Moreover, photodecomposition of complex **5** could be also triggered upon irradiation at 810 nm, *i.e.* in the NIR region. All complexes release CO upon irradiation, as proven by the myoglobin assay. Our approach provides a chemical process for the systematic preparation of photoCORMs triggered by low-power red light. We believe that this approach could be generalized for further development of photoCORMs.

Experimental

General experimental details

Reagents were purchased from commercial sources and used as received. ^{1}H-NMR and ^{13}C-NMR were performed on Bruker Avance III spectrometers operating at 400 or 500 MHz (as specified for each molecule). High resolution mass spectra were measured with a Bruker FTMS 4.7 T BioAPEXII spectrometer. IR spectra were measured with a Bruker Tensor 27. UV-Vis spectroscopy was performed using a Perkin-Elmer Lambda 35. Irradiation at λ_{max} (vis.) was performed using an Edinburgh FS5 fluorimeter (excitation slit: 1 nm) equipped with a 150 W Xe lamp. Qualitative evidence of CO evolution was obtained *via* myoglobin (Mb) assay. Solutions of the complexes were prepared in DMSO and added in a 1 : 1 molar ratio to a 20 μM solution of reduced horse heart Mb. Photodecomposition kinetics were calculated upon fitting of the mono-exponential decay by using the software Origin 7.5 (examples are given in Fig. S14†).

Crystallographic data were collected with Mo-Kα radiation (λ = 0.71073 Å). All measurements were performed at 200 K with Stoe IPDS-II or IPDS-II T diffractometers equipped with Oxford Cryosystem open-flow cryostats.[32] The crystals were mounted on loops, and all geometric and intensity data were obtained from these crystals. The absorption corrections were partially integrated in the data reduction procedure.[33] The structures were solved and refined by full-matrix least-squares techniques on F^2 with the SHELX 2014 package.[34] All atoms (except hydrogen atoms) were refined anisotropically. Hydrogen atoms were introduced as fixed contributors if a residual electronic density was observed near their expected positions. CCDC 1430147 (for Azpy_CF3), 1430146 (for Azpy_CF_3Cl), 1446608 (for Azpy_Br), 1430149 (for **2**), and 1430148 (for **2a**), contain the supplementary crystallographic data for this paper.

Geometry optimizations and molecular orbital calculations were performed using DFT methods. A B3LYP functional was used with a 6-31G* basis set. Mn was modelled with a LANL2DZ effective core basis set. The optimised structures were verified *via* frequency calculations, which showed the absence of imaginary frequencies. Electronic transitions were modelled by TD-DFT methods using the same functional and basis set. The electronic transition with the highest oscillator strength (>0.015) in the visible region was selected for comparison with the experimental lowest energy band (λ_{max} (vis.)). All calculations were performed with Spartan 14 software.

General synthesis of 2,2′-azopyridines ligands

A suitable amount of 2-aminopyridine was dissolved in 5 ml of THF and added to 10 ml of NaOCl (13% aqueous solution). THF was removed under vacuum without heating and the resulting red suspension was stirred overnight. The mixture was diluted with 50 ml of water and extracted 3 times with 10 ml of EtOAc. The organic phases were collected, washed with brine and dried over Na_2SO_4. The solvent was removed and the crude product was purified by column chromatography (SiO_2, eluents and yields are given for each compound).

1,2-Bis(4-methylpyridin-2-yl)diazene (Azpy_Me). 500 mg (4.6 mmol) of 4-methylpyridin-2-amine were reacted according to the general procedure. Eluent mixture: $CHCl_3$: MeOH (10% NH_4OH) 98 : 2. Yield: 60 mg, 12%. Anal. Calc. for $C_{12}H_{12}N_4$: C, 67.90; H, 5.70; N, 26.40%. Found: C, 67.71; H, 5.67; N, 27.00%. ^{1}H-NMR (400 MHz, CD_2Cl_2): δ (ppm) 8.59–8.60 (d, J = 4.5 Hz, 2H, 2 × CH), 7.69 (s, 2H, 2 × CH), 7.29–7.30 (d, J = 4.5 Hz, 2H, 2 × CH), 2.48 (s, 6H, 2 × CH_3). ^{13}C-NMR (100 MHz, CD_2Cl_2): δ (ppm) 164, 150, 150, 127, 115, 21. HR-ESI (m/z): calc. 213.1140 ($C_{12}H_{13}N_4$, $[M + H]^+$) exp. 213.1131.

1,2-Di(pyridin-2-yl)diazene (Azpy_H). 1 g (10.6 mmol) of 2-aminopyridine was dissolved in 20 mL of water. 50 mL of NaClO 13% was then added at 10 °C and the reaction mixture was stirred overnight at room temperature. The solution was then extracted three times with diethylether, the organic phases were collected and dried over Na_2SO_4 and the solvents were removed. The red-orange powder was then dissolved in a minimal amount of petroleum ether and kept at 4 °C for crystallization. The resulting solid was filtered giving 760 mg (50%) of the pure product. Anal. Calc. for $C_{10}H_8N_4$: C, 65.21; H, 4.38; N, 30.42%. Found: C, 64.95; H, 4.90; N, 30.32%. ^{1}H-NMR (400 MHz, CD_2Cl_2): δ (ppm): 8.78–8.79 (dd, J = 1.0 Hz, J = 4.8 Hz, 2H, 2 × CH), 7.99–8.03 (dt, J = 1.9 Hz, J = 7.5 Hz, 2H, 2 × CH), 7.92–7.94 (d, J = 6.1 Hz, 2H, 2 × CH), 7.52–7.56 (ddd, J = 1.1 Hz, J = 4.8 Hz, J = 7.4 Hz, 2H, 2 × CH). ^{13}C-NMR (125 MHz CD_2Cl_2): δ (ppm) 163, 150, 138, 126, 114. HR-ESI (m/z): calc. 185.0749 ($C_{10}H_8N_4$, $[M + H]^+$) exp. 185.0821.

1,2-Bis(4-bromopyridin-2-yl)diazene (Azpy_Br). 350 mg (2 mmol) of 2-amino-4-bromopyridine were reacted according to the general procedure. Eluent mixture: CH_2Cl_2 : MeOH 50 : 1. Yield: 35 mg, 10%. Anal. Calc. for $C_{10}H_6N_4Br_2$: C, 35.12; H, 1.77; N, 16.38%. Found: C, 34.91; H, 2.34; N, 16.19%. ^{1}H-NMR (400 MHz, CD_2Cl_2): δ (ppm) 8.60–8.61 (d, J = 5.1 Hz, 2H, 2 × CH), 8.05–8.06 (d, J = 1.7 Hz, 2H, 2 × CH), 7.67–7.68 (dd, J = 1.8 Hz, J = 5.3 Hz, 2H, 2 × CH). ^{13}C-NMR (125 MHz CD_2Cl_2): δ (ppm) 163, 150, 134, 129, 117. HR-ESI (m/z): calc. 342.9012 ($C_{10}H_6N_4Br_2$, $[M + H]^+$) exp. 342.9013.

1,2-Bis(4-(trifluoromethyl)pyridin-2-yl)diazene (Azpy_CF_3). 1 g (6.17 mmol) of 4-(trifluoromethyl)pyridine-2-amine was reacted according to the general procedure. Eluent mixture: CH_2Cl_2 : MeOH (10% NH_4OH) 98 : 2. Yield: 400 mg, 40%. Anal. Calc. for $C_{12}H_6F_6N_4$: C, 45.01; H, 1.89; N, 17.50%. Found: C, 44.97; H, 2.20; N, 17.24%. ^{1}H-NMR (400 MHz, CD_2Cl_2): δ (ppm) 8.98–8.99 (d, J = 2.0 Hz, 2H, 2 × CH), 8.15 (s, 2H), 7.75–7.76 (d, J = 2.0 Hz, 2H, 2 × CH). ^{13}C-NMR (100 MHz, CD_2Cl_2): δ (ppm) 163, 151, 141, 141, 122, 110. HR-ESI (m/z): calc. 321.0575 ($C_{12}H_7F_6N_4$, $[M + H]^+$) exp. 321.0562.

1,2-Bis(5-chloro-4-(trifluoromethyl)pyridin-2-yl)diazene (Azpy_CF_3Cl). This ligand was obtained as a side product from the reaction used for Azpy_CF_3 using the same eluent mixture. Yield: 70 mg, 6%. Anal. Calc. for $C_{12}H_4Cl_2F_6N_4$: C, 37.04; H, 1.04; N, 14.40%. Found: C, 37.01; H, 0.99; N, 14.21%. ^{1}H-NMR (400 MHz, CD_2Cl_2): δ (ppm) 8.94 (s, 2H, 2 × CH), 8.22 (s, 2H, 2 × CH). ^{13}C-NMR (100 MHz, CD_2Cl_2): δ (ppm) 161, 152, 132, 123, 113. HR-ESI (m/z): calc. 388.9795 ($C_{12}H_5Cl_2F_6N_4$, $[M + H]^+$) exp. 388.9790.

General synthesis of Mn complexes

Because of the light sensitivity of the complexes, the synthesis and purification of such compounds must be performed in the dark. 30 mg of a suitable ligand were dissolved in dry CH_2Cl_2. The solution was degassed with 3 Ar/vacuum cycles and 3 equivalents of $Mn(CO)_5Br$ were added. The mixture was then degassed again with 3 Ar/vacuum cycles and stirred for 3 h in the dark at room temperature. The solvent was carefully removed under vacuum at room temperature and the resulting solid was dissolved in pentane : CH_2Cl_2 1 : 1 and purified by dry flash chromatography. After a first elution with 3 fractions of 5 ml each of pentane : CH_2Cl_2 1 : 1 (to remove the excess of $Mn(CO)_5Br$, the target complexes were eluted 3 times with 5 ml fractions of final eluent (see the synthesis of each compound for details)). The fractions were collected and the solvent was removed under vacuum in the dark at room temperature. Unless specified, all complexes were synthesized according to this general procedure.

***fac*-[Mn(CO)$_3$(Azpy_Me)Br] (1).** Eluent: CH_2Cl_2. Yield: 21 mg, 34%. Anal. Calc. for $C_{15}H_{12}BrMnN_4O_3$: C, 41.79; H, 2.81; N, 13.00%. Found: C, 42.15; H, 2.79; N, 13.50%. ^{1}H-NMR (500 MHz, CD_2Cl_2): δ (ppm) 9.02–9.03 (d, J = 7.0 Hz, 1H, CH), 8.62–8.63 (d, J = 6.5 Hz, 1H, CH), 8.55 (s, 1H, CH), 7.78 (d, J = 1.0 Hz, 1H, CH), 7.43–7.47 (t, J = 9.0 Hz, J = 15.5 Hz 2H, 2 × CH), 2.67 (s, 3H, CH_3), 2.54 (s, 3H, CH_3). ^{13}C-NMR (125 MHz, CD_2Cl_2): δ (ppm) 165, 164, 152, 151, 151, 148, 130, 128, 128, 115, 21, 21. The measurement of HR-ESI was not possible due to decomposition of the product. IR: ν = 2028 cm^{-1}, 1945 cm^{-1} (νCO stretchings).

***fac*-[Mn(CO)$_3$(Azpy_H)Br] (2).** In the dark, 36 mg (0.22 mmol) of Azpy_H were dissolved in 5 mL of DCM. 60.2 mg (0.66 mmol, 3 eq.) of $Mn(CO)_5Br$ were then added and the reaction mixture was stirred overnight in the dark at room temperature. The dark blue solution was dried and washed three times with hexane. The remaining blue solid was redissolved in a minimal amount of DCM and hexane was laid on top. The obtained crystals were dried on the vacuum line. Yield: 23 mg, 28%. Anal. Calc. for $C_{13}H_8BrMnN_4O_3$: C, 38.74; H, 2.00; N, 13.90%. Found: C, 38.00; H, 2.20; N, 13.82%. ^{1}H-NMR (500 MHz, CD_2Cl_2): δ (ppm) 9.22–9.24 (d, J = 4.8 Hz, 1H, CH), 8.79–8.80 (d, J = 4.7 Hz, 1H, CH), 8.66–8.68 (d, J = 17.9 Hz, 1H, CH), 8.20–8.24 (t, J = 7.8 Hz, 1H, CH), 8.01–8.02 (d, J = 4.5 Hz, 2H, 2 × CH), 7.61–7.67 (m, J = 6.1 Hz, J = 26.1 Hz, 2H, 2 × CH). ^{13}C-NMR (125 MHz, CD_2Cl_2): δ (ppm) 165,

163, 152, 148, 139, 139, 130, 128, 127, 114. The measurement of HR-ESI was not possible due to decomposition of the product. IR: ν = 2024 cm^{-1}, 1922 cm^{-1} (νCO stretchings).

***fac*-[Mn(CO)$_3$(Azpy_Br)Br] (3).** Eluent: CH_2Cl_2. Yield: 5 mg, 10%. ^{1}H-NMR (500 MHz, CD_2Cl_2): δ (ppm) 8.99–9.00 (d, J = 5.8 Hz, 1H, CH), 8.83–8.84 (d, J = 2.4 Hz, 1H, CH), 8.61–8.62 (d, J = 5.3 Hz, 1H, CH), 8.21 (d, J = 2 Hz, 1H, CH), 7.82–7.84 (dd, J = 5.0 Hz, 1H, CH), 7.77–7.79 (d, J = 6.0 Hz, 1H, CH). ^{13}C-NMR (125 MHz, CD_2Cl_2): δ (ppm) 168, 165, 152, 149, 133, 130, 129, 117. The measurement of HR-ESI was not possible due to the thermal decomposition of the product. IR: ν = 2030 cm^{-1}, 1938 cm^{-1} (νCO stretchings).

***fac*-[Mn(CO)$_3$(Azpy_CF$_3$)Br] (4).** Eluent mixture: pentane : CH_2Cl_2 3 : 7. Yield: 5 mg, 10%. ^{1}H-NMR (500 MHz, CD_2Cl_2): δ (ppm) 9.42–9.43 (d, J = 6.5 Hz, 1H, CH), 8.99–9.00 (d, J = 4.5 Hz, 1H, CH), 8.64 (s, 1H, CH), 8.36 (s, 1H, CH), 7.93–7.94 (d, J = 5.5 Hz, 1H, CH), 7.84–7.86 (d, J = 6.5 Hz, 1H, CH). ^{13}C-NMR (125 MHz, CD_2Cl_2): δ (ppm) 165, 163, 153, 150, 141, 141, 126, 124, 122, 121, 111. The measurement of HR-ESI was not possible due to the thermal decomposition of the product. IR: ν = 2032 cm^{-1}, 1930 cm^{-1} (νCO stretchings).

***fac*-[Mn(CO)$_3$(Azpy_CF$_3$Cl)Br] (5).** Eluent mixture: pentane : CH_2Cl_2 4 : 6. Yield: 3 mg, 7%. ^{1}H-NMR (500 MHz, CD_2Cl_2): δ (ppm) 9.38 (s, 1H, CH), 8.94–8.95 (d, J = 4.5 Hz, 2H, 2 × CH), 8.45 (s, 1H, CH). The measurement of HR-ESI and ^{13}C-NMR was not possible due to the thermal decomposition of the product. IR: ν = 2036 cm^{-1}, 1928 cm^{-1} (νCO stretchings).

Note: Complexes **4** and **5** (and to a lesser extent **3**) are thermally unstable both in the solid state and in solution. However in the solid state the compounds can be stored for several months at −20 °C and for a few days in DCM solutions.

Acknowledgements

Financial support from the Swiss National Science Foundation (Grant# PP00P2_144700) is gratefully acknowledged. The authors are thankful to Felix Fehr (University of Fribourg) for NMR measurements.

Notes and references

1 R. Mede, M. Klein, R. A. Claus, S. Krieck, S. Quickert, H. Görls, U. Neugebauer, M. Schmitt, G. Gessner, S. H. Heinemann, J. Popp, M. Bauer and M. Westerhausen, *Inorg. Chem.*, 2016, **55**, 104–113.
2 U. Schatzschneider, *Br. J. Pharmacol.*, 2015, **172**, 1638–1650.
3 S. Garcia-Gallego and G. J. L. Bernardes, *Angew. Chem., Int. Ed.*, 2014, **53**, 9712–9721.
4 C. C. Romao, W. A. Blättler, J. D. Seixas and G. J. Bernardes, *Chem. Soc. Rev.*, 2012, **41**, 3571–3583.
5 F. Zobi, *Future Med. Chem.*, 2013, **5**, 175–188.
6 E. Stamellou, D. Storz, S. Botov, E. Ntasis, J. Wedel, S. Sollazzo, B. K. Kramer, W. van Son, M. Seelen, H. G. Schmalz, A. Schmidt, M. Hafner and B. A. Yard, *Redox Biol.*, 2014, **2**, 739–748.
7 S. Romanski, B. Kraus, U. Schatzschneider, J. M. Neudorfl, S. Amslinger and H. G. Schmalz, *Angew. Chem., Int. Ed.*, 2011, **50**, 2392–2396.
8 N. S. Sitnikov, Y. C. Li, D. F. Zhang, B. Yard and H. G. Schmalz, *Angew. Chem., Int. Ed.*, 2015, **54**, 12314–12318.
9 U. Schatzschneider, *Inorg. Chim. Acta*, 2011, **374**, 19–23.
10 R. D. Rimmer, A. E. Pierri and P. C. Ford, *Coord. Chem. Rev.*, 2012, **256**, 1509–1519.
11 J. Marhenkea, K. Trevinob and C. Works, *Coord. Chem. Rev.*, 2016, **306**, 533–543.
12 S. J. Carrington, I. Chakraborty, J. M. L. Bernard and P. K. Mascharak, *ACS Med. Chem. Lett.*, 2014, **5**, 1324–1328.
13 V. Yempally, S. J. Kyran, R. K. Raju, W. Y. Fan, E. N. Brothers, D. J. Darensbourg and A. A. Bengali, *Inorg. Chem.*, 2014, **53**, 4081–4088.
14 H. T. Poh, B. T. Sim, T. S. Chwee, W. K. Leong and W. Y. Fan, *Organometallics*, 2014, **33**, 959–963.
15 F. Zobi, L. Quaroni, G. Santoro, T. Zlateva, O. Blacque, B. Sarafimov, M. C. Schaub and A. Y. Bogdanova, *J. Med. Chem.*, 2013, **56**, 6719–6731.
16 J. S. Ward, J. M. Lynam, J. Moir and I. J. S. Fairlamb, *Chem. – Eur. J.*, 2014, **20**, 15061–15068.
17 J. S. Ward, J. M. Lynam, J. W. B. Moir, D. E. Sanin, A. P. Mountford and I. J. S. Fairlamb, *Dalton Trans.*, 2012, **41**, 10514–10517.
18 I. Chakraborty, S. J. Carrington and P. K. Mascharak, *Acc. Chem. Res.*, 2014, **47**, 2603–2611.
19 M. A. Gonzalez, M. A. Yim, S. Cheng, A. Moyes, A. J. Hobbs and P. K. Mascharak, *Inorg. Chem.*, 2012, **51**, 601–608.
20 S. J. Carrington, I. Chakraborty and P. K. Mascharak, *Chem. Commun.*, 2013, **49**, 11254–11256.
21 S. J. Carrington, I. Chakraborty and P. K. Mascharak, *Dalton Trans.*, 2015, **44**, 13828–13834.
22 M. A. Gonzales and P. K. Mascharak, *J. Inorg. Biochem.*, 2014, **133**, 127–135.
23 L. Flamigni, A. Barbieri, C. Sabatini, B. Ventura and F. Barigelletti, *Top. Curr. Chem.*, 2007, **281**, 143–203.
24 R. A. Kirgan, B. P. Sullivan and D. P. Rillema, *Top. Curr. Chem.*, 2007, **281**, 45–100.
25 M. A. Gonzalez, S. J. Carrington, N. L. Fry, J. L. Martinez and P. K. Mascharak, *Inorg. Chem.*, 2012, **51**, 11930–11940.
26 A. J. Atkin, J. M. Lynam, B. E. Moulton, P. Sawle, R. Motterlini, N. M. Boyle, M. T. Pryce and I. J. S. Fairlamb, *Dalton Trans.*, 2011, **40**, 5755–5761.
27 S. McLean, B. E. Mann and R. K. Poole, *Anal. Biochem.*, 2012, **427**, 36–40.
28 W. W. Fang, X. Y. Liu, Z. W. Lu and T. Tu, *Chem. Commun.*, 2014, **50**, 3313–3316.
29 Y. Takeda, S. Okumura and S. Minakata, *Synthesis*, 2013, 1029–1033.

30 T. M. Klapotke and D. G. Piercey, *Inorg. Chem.*, 2011, **50**, 2732–2734.
31 A. E. Pierri, P. J. Huang, J. V. Garcia, J. G. Stanfill, M. Chui, G. Wu, N. Zheng and P. C. Ford, *Chem. Commun.*, 2015, **51**, 2072–2075.
32 J. Cosier and A. M. Glazer, *J. Appl. Crystallogr.*, 1986, **19**, 105–107.
33 E. Blanc, D. Schwarzenbach and H. D. Flack, *J. Appl. Crystallogr.*, 1991, **24**, 1035–1041.
34 G. M. Sheldrick, *Acta Crystallogr., Sect. A: Fundam. Crystallogr.*, 2008, **64**, 112–122.